

THE JOURNAL OF PHYSICAL CHEMISTRY B

Subscriber access provided by UNIVERSITY OF TOLEDO LIBRARIES

B: Glasses, Colloids, Polymers, and Soft Matter

Structural Characterization of Biocompatible Reverse Micelles using Small-Angle X-Ray Scattering, P Nuclear Magnetic Resonance and Fluorescence Spectroscopy

Emmanuel Odella, Ruben Dario Falcone, Marcelo Ceolin, Juana J. Silber, and N. Mariano Correa

J. Phys. Chem. B, **Just Accepted Manuscript** • DOI: 10.1021/acs.jpcc.7b11395 • Publication Date (Web): 28 Mar 2018Downloaded from <http://pubs.acs.org> on March 28, 2018

Just Accepted

“Just Accepted” manuscripts have been peer-reviewed and accepted for publication. They are posted online prior to technical editing, formatting for publication and author proofing. The American Chemical Society provides “Just Accepted” as a service to the research community to expedite the dissemination of scientific material as soon as possible after acceptance. “Just Accepted” manuscripts appear in full in PDF format accompanied by an HTML abstract. “Just Accepted” manuscripts have been fully peer reviewed, but should not be considered the official version of record. They are citable by the Digital Object Identifier (DOI®). “Just Accepted” is an optional service offered to authors. Therefore, the “Just Accepted” Web site may not include all articles that will be published in the journal. After a manuscript is technically edited and formatted, it will be removed from the “Just Accepted” Web site and published as an ASAP article. Note that technical editing may introduce minor changes to the manuscript text and/or graphics which could affect content, and all legal disclaimers and ethical guidelines that apply to the journal pertain. ACS cannot be held responsible for errors or consequences arising from the use of information contained in these “Just Accepted” manuscripts.



ACS Publications

is published by the American Chemical Society, 1155 Sixteenth Street N.W.,
Washington, DC 20036Published by American Chemical Society. Copyright © American Chemical Society.
However, no copyright claim is made to original U.S. Government works, or works
produced by employees of any Commonwealth realm Crown government in the course
of their duties.

1
2
3 ***Structural Characterization of Biocompatible Reverse Micelles using***
4
5 ***Small-Angle X-Ray Scattering, ³¹P Nuclear Magnetic Resonance and***
6
7 ***Fluorescence Spectroscopy***
8
9

10
11
12 Emmanuel Odella,^{*†a} R. Darío Falcone,[†] Marcelo Ceolín,[§] Juana J. Silber[†] and N.

13
14 Mariano Correa^{†*}
15
16
17
18
19
20

21 [†] *Departamento de Química. Universidad Nacional de Río Cuarto. Agencia Postal # 3.*

22
23 *C.P. X5804BYA, Río Cuarto, Argentina.*
24

25 [§] *Instituto de Investigaciones Fisicoquímicas Teóricas y Aplicadas. UNLP-CONICET*

26
27 *(CCT-La Plata) Diagonal 113 y 64 (B1906ZAA), La Plata, Argentina.*
28

29 ^a *Current address: School of Molecular Sciences, Arizona State University, Tempe,*

30
31 *Arizona 85287, United States.*
32
33
34
35
36
37
38
39

40 [*] Dr. N. Mariano Correa, Dr. Emmanuel Odella Corresponding-Authors, E-mails:

41 mcorrea@exa.unrc.edu.ar; eodella@asu.edu
42
43
44
45
46
47
48
49
50
51
52
53
54
55
56
57
58
59
60

1
2
3 **ABSTRACT:** The most critical problem regarding the use of reverse micelles (RMs) in
4 several fields is the toxicity of their partial components. In this sense, many efforts have
5 been made to characterize non-toxic RMs formulations based on biological amphiphiles
6 and/or different oils. In this contribution, the microstructure of biocompatible mixed
7 RMs formulated by sodium 1,4-bis-2-ethylhexylsulfosuccinate (AOT) and tri-*n*-
8 octylphosphine oxide (TOPO) surfactants dispersed in the *friendly solvent* methyl
9 laurate was studied by using SAXS, ³¹P NMR and, following the solvatochromic
10 behavior of the molecular probe 4-aminophthalimide (4-AP). The results indicated the
11 presence of RMs aggregates on TOPO incorporation with a droplet size reduction, and
12 an increase on the interfacial fluidity in comparison with pure AOT RMs. When
13 confined inside the mixed systems 4-AP showed red-edge excitation shift and confirms
14 the increment of interfacial fluidity upon TOPO addition. Also, the partition between
15 the external nonpolar solvent and the RMs interface, and an increase in both the local
16 micropolarity and the capability to form hydrogen bond interaction between 4-AP and
17 mixed interface were observed. The findings have been explained in terms of the
18 nonionic surfactant structure and its complexing nature expressed at interfacial level.
19 Notably, we show how two different approaches, i.e. SAXS and the solvatochromism of
20 the probe 4-AP, can be used in a complementary way to enhance our understanding of
21 the interfacial fluidity of RMs, parameter that is difficult to measure directly.
22
23
24
25
26
27
28
29
30
31
32
33
34
35
36
37
38
39
40
41
42
43
44
45
46
47
48
49
50
51
52
53
54
55
56
57
58
59
60

INTRODUCTION

The use and impact of reverse micelles (RMs) have been of growing interest during the past decade in both academic and technological applications. Properties such as their small size, thermodynamic stability, dynamic character, optical transparency and the peculiar interactions between the interface and the confined solvents are the key for chemical reactions,¹⁻³ enzymatic reactions⁴⁻⁸ and nanoparticle synthesis^{9,10} performed inside them. RMs are spatially ordered macromolecular assemblies of surfactants formed in nonpolar solvents, in which the polar head groups of the surfactants point inward toward a polar core and the hydrocarbon chains point outward toward the nonpolar medium.¹¹⁻¹³ The potential application of highly biocompatible aqueous RMs to food, cosmetic, and pharmaceutical industry as solubilization media of hydrophilic, hydrophobic, and amphiphilic functional materials displayed growing interest during the last years.¹⁴⁻¹⁸ Undoubtedly the most critical problem regarding a biocompatible use of RMs is the potential toxicity of their partial components. In these sense, many efforts have been made to characterize non-toxic RMs formulations based on biological amphiphiles and/or different oils. In particular, RMs systems dissolved in isopropyl myristate (IPM), ethyl myristate (EM), ethyl palmitate (EP) and ethyl oleate (EO) are quite promising.¹⁴⁻¹⁹ These long chain fatty acid esters are environmentally friendly with low toxicity and highly biodegradable, and most interestingly they show structural resemblance with the lipids in living systems.¹⁹⁻²²

On the other hand, it has been found that the addition of nonionic surfactants to the RMs interfaces formed by ionic surfactants, produces significant changes in water solubilization, droplet sizes as well as modifies the water or polar solvents structure inside the nanopool.^{20,23-25} Kundu et. al.^{20,21} explored the influence of nonionic surfactant Tween-85 on the properties of anionic sodium 1,4-bis-2-

1
2 ethylhexylsulfosuccinate (AOT) based micelle as well as RMs in fatty acid esters (EM,
3 EP and EO). A comprehensive investigation of the micellization behavior at different
4 mixed molar fraction of Tween-85 ($X_{\text{Tween-85}}$) was made by surface tension methods.
5
6 Non-ideal mixing behaviors along with synergistic interaction between the constituent
7 surfactants in the mixed micelles were evidenced. Also, mixed micelles illustrate
8 favorable micellization behavior in terms of thermodynamic parameters, and fatty acid
9 ester medium-based mixed RMs shows synergism in water solubilization capacity. Das
10 et. al.⁶ studied the effect of replacing AOT by nonionic surfactant(s) of varying
11 hydrophilic-lipophilic balance (HLB) on the structure, dynamics and activity of water
12 encapsulated in RMs formed in IPM. Furthermore, they measured the enzymatic
13 activity of α -chymotrypsin on the substrate Ala-Ala-Phe-7-amido-4-methyl coumarin
14 and found that the enzymatic rate could either be enhanced or reduced depending on the
15 HLB of the nonionic surfactant. Bardhan et. al.²⁶ studied the mixed
16 cetyltrimethylammonium bromide and polyoxyethylene (23) lauryl ether
17 microemulsions stabilized in 1-pentanol and IPM. The formation of mixed surfactant
18 microemulsions was found to be spontaneous at all compositions, whereas it was
19 endothermic at equimolar composition.
20
21
22
23
24
25
26
27
28
29
30
31
32
33
34
35
36
37
38

39 As summarized, there is clear evidence that the properties of RMs are modified
40 when composed of mixed surfactants. However, to the best of our knowledge, all the
41 studies are performed using nonionic surfactants which have a very long polar part in
42 their moiety. Besides, most of those investigations are not focused on understanding one
43 important parameter such as the fluidity of the interface. In view of the above, the
44 present study aims at a precise characterization of the mixed systems formed by the
45 AOT and the nonionic surfactant tri-*n*-octyl phosphine oxide (TOPO) dissolved in the
46 friendly solvent methyl laurate (ML). In particular, TOPO has a very small polar head
47
48
49
50
51
52
53
54
55
56
57
58
59
60

1
2
3 (the P=O group) in comparison with its hydrophobic chains, and has more than one
4 hydrocarbon tail and distinguishes from those that have only a single tail. Furthermore,
5 the great versatility in the use of TOPO in different fields lies in the complexing
6 properties of the P=O group.²⁷⁻³⁰
7
8
9

10
11 Previous studies performed in our group¹⁸ have shown very peculiar and
12 interesting water properties inside AOT RMs formed in ML, and compared with the
13 systems dispersed in IPM. The droplets size values, the maximum amount of water
14 solubilized and the aggregation number (N_{agg}) of both AOT RMs are dissimilar
15 considering the chemical structure of the external solvents and they can be explained
16 taking into account the different non-polar solvent penetration to the interface. We have
17 also characterized the mixed system formed with AOT and TOPO in *n*-heptane, and
18 found interesting properties in both the micellar interface and the confined water
19 behavior.^{27,30} We demonstrated both the existence of “bulk-like” water molecules at
20 small W_0 values and the reduction of the mixed RMs size upon TOPO addition.
21
22
23
24
25
26
27
28
29
30
31

32
33 In this contribution we have investigated by different techniques such as small
34 angle X-ray scattering (SAXS) and ³¹P NMR spectroscopy, the size and morphology of
35 the mixed RMs dispersed in ML, and the different molecular interactions between water
36 and the mixed interface at W_0 ($W_0 = [H_2O]/([AOT] + [TOPO])$)=2. In addition, we have
37 introduced the molecular probe 4-aminophthalimide (4-AP) to explore the different
38 environment properties. It is known that 4-AP is an excellent probe because its
39 fluorescence lifetimes, spectra and quantum yields are affected greatly by its
40 microenvironment.³¹⁻³³ We want to take advantages of the dependence of the emission
41 band with the excitation wavelength in order to investigate complex systems like mixed
42 RMs.
43
44
45
46
47
48
49
50
51
52
53

1
2
3 The results show that by increasing the molar fraction of TOPO
4 ($X_{\text{TOPO}} = [\text{TOPO}] / ([\text{AOT}] + [\text{TOPO}])$), the water solubilization capacity diminished
5 drastically. SAXS experiments show that mixed RMs at $W_0=2$ are formed
6 spontaneously in every AOT:TOPO mixture investigated, and the droplet sizes decrease
7 as the TOPO content increase. The data also suggest an increase on the droplets fluidity
8 and the presence of the RMs aggregates at higher X_{TOPO} . The probe 4-AP undergoes a
9 partition process between the external nonpolar solvent and the RMs interface and, this
10 feature was used to obtain the “operational” critical micellar concentration (cmc_{op}) of
11 every system investigated. Also, the solvatochromic study of 4-AP shows that the probe
12 is capable of monitoring both an increase in the local micropolarity and, the capability
13 to form hydrogen bond (H-bond) interaction between 4-AP and mixed interface when
14 X_{TOPO} increases. Thus, we demonstrate the mixed RMs formation using the friendly ML
15 solvent and, how the TOPO addition changes considerably the RMs properties,
16 especially the interfacial fluidity. Under this perspective, the present mixed surfactants
17 systems combine the unique characteristics of the water confined into AOT RMs and
18 the complexity features of TOPO surfactant, in order to generate a special soft-template
19 for nanoparticles synthesis, a venue that we are currently investigating.
20
21
22
23
24
25
26
27
28
29
30
31
32
33
34
35
36
37
38
39
40

41 **EXPERIMENTAL SECTION**

42
43
44 **Materials:** Sodium 1,4-bis (2-ethylhexyl) sulfosuccinate (AOT) and tri-*n*-octyl
45 phosphine oxide (TOPO) were purchased from Sigma and were dried under vacuum
46 prior use. Methyl Laurate (ML) from Sigma (HPLC quality), was used without
47 purification and stored over molecular sieves (4 Å) before use. The molecular probe 4-
48 aminophthalimide (4-AP) from Sigma was purified by repeated recrystallization from
49
50
51
52
53
54
55
56
57
58
59
60

1
2 ethanol.³¹ Doubly distilled water of conductivity less than 5 $\mu\text{S cm}^{-1}$ was used in the
3
4
5 experiments.

6
7 **Methods:** AOT and TOPO were individually dissolved in ML at a concentration
8
9 of 0.25 M to prepare the respective stock solutions and then mixed in the desired
10 proportions. The X_{TOPO} was varied from 0 to 1 in water solubilization capacity
11 experiments and from 0 to 0.7 for both SAXS and spectroscopic experiments in the
12 mixed systems. Aliquots of these stock solutions were used to make individual mixed
13
14 RMs solutions with different water contents (W_0). Water was incorporated into each
15 micellar solutions by using calibrated microsyringes. The solutions were agitated in a
16
17 sonicating bath until the microemulsion was optically clear. A stock solution of 4-AP
18 (1×10^{-3} M) was prepared in acetonitrile (Sintorgan, HPLC quality). The appropriate
19 amount of this solution to achieve a final concentration of 1×10^{-4} M of the probe in the
20 micellar medium was transferred into a volumetric flask, and the solvent was
21 evaporated by bubbling dry N_2 ; then ML was added to the residue and the resulting
22 solution was used to prepare the surfactants containing samples. To a cell containing 2
23 mL of 4-AP (1×10^{-4} M) in ML were added different amounts of surfactant and
24
25 molecular probe stock solutions to obtain a given concentration of surfactant in the
26 micelle media. Therefore, the absorption and emission of the probe were not affected by
27
28 dilution. The lowest value for W_0 ($W_0=0$) corresponds to a system without the water
29 addition.

30
31
32
33
34
35
36
37
38
39
40
41
42
43
44
45
46 **General.** SAXS experiments were performed at INIFTA (La Plata, Argentina,
47 project "Nanopymes", EuropeAid/132184/D/SUP/AR-Contract 331-896) facilities
48 using a XEUSS 1.0 equipment from XENOCSS with a $K\alpha$ -Cu radiation microsource
49 ($\lambda=0.154$ nm). A PILATUS-100K detector was used with 543.4 mm sample to detector
50 distance, which was calibrated using silver behenate. One-dimensional curves were
51
52
53
54
55
56
57

obtained by integration of the 2D data using the Foxtrot program (software developed on the SWING beamline).³⁴ The scattering intensity distributions as a function of the scattering vector (q) were obtained in the q range between 0.056 and 0.500 \AA^{-1} . The samples were placed in borosilicate glass capillary tubes of 1.5 mm of diameter and 10 μm of wall thickness. The scattering data were corrected for the background scattering from both the capillary tubes and the ML solvent. Data was analyzed using the indirect transformation procedure of Glatter.³⁵ The pair distance distribution function $\rho(r)$ was obtained by Fourier transform of the scattering intensity $I(q)$ as:

$$\rho(r) = \frac{1}{2\pi^2} \int_0^\infty r q I(q) \sin(qr) dq \quad (1)$$

$$q = \frac{4\pi}{\lambda} \sin \frac{\theta}{2} \quad (2)$$

where q is the amplitude of the scattering vector, θ and λ are the scattering angle and the X-ray wavelength, respectively, and r is the distance in real space. The $\rho(r)$ function depends on the particle geometry and on the inner heterogeneity of the scattering density distribution in the particle, and their shape directly reflects the form of the RMs droplets.³⁶ The gyration radius (R_g) was calculated in two ways: (i) by using the Guinier plot (eq (4)) on the data sets in a defined small q range ($q \rightarrow 0$), we determined the value of R_g by using the Guinier's law:³⁵

$$I(q)_{q \rightarrow 0} = I_0 e^{-\left(\frac{q^2 R_g^2}{3}\right)} \quad (3)$$

$$\ln I(q)_{q \rightarrow 0} = \ln I_0 - \frac{q^2 R_g^2}{3} \quad (4)$$

(ii) by using the following equation:³⁶

$$R_{g,r}^2 = \frac{\int_0^{D_{\max}} \rho(r)r^2 dr}{2 \int_0^{D_{\max}} \rho(r) dr} \quad (5)$$

where D_{\max} is the maximum diameter of the particle, which is estimated from the $\rho(r)$ function satisfying the condition $\rho(r)=0$ for $r>D_{\max}$. In eq (5), $R_{g,r}$ means that the determination was in real space.

We have also performed ^{31}P NMR, steady state absorption and emission spectroscopy measurements. The instrumentation section is discussed in the supporting information (SI) in detail (section 2).

RESULTS AND DISCUSSIONS

1. Water Solubilization Capacity (W_0^{\max}). Water solubilization capacity (W_0^{\max}) of AOT:TOPO mixed systems (at $X_{\text{TOPO}}=0 \rightarrow 1.0$) in ML at 25.0 °C are presented in Figure 1. Single AOT system ($X_{\text{TOPO}}=0$) has been observed to solubilize a substantial amount of water, $W_0^{\max} \sim 43$ which is consistent with the literature reports.¹⁸ When the X_{TOPO} increases, the W_0^{\max} diminishes dramatically until $W_0^{\max} \sim 1$ for single TOPO/ML system.

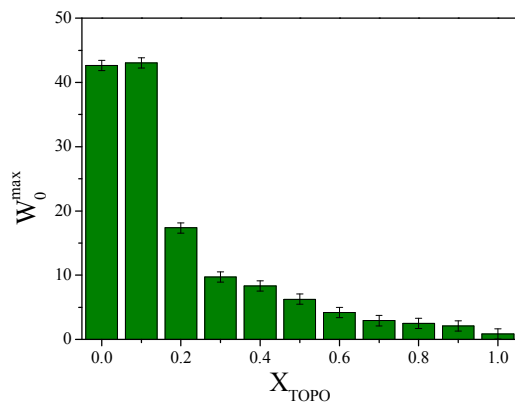
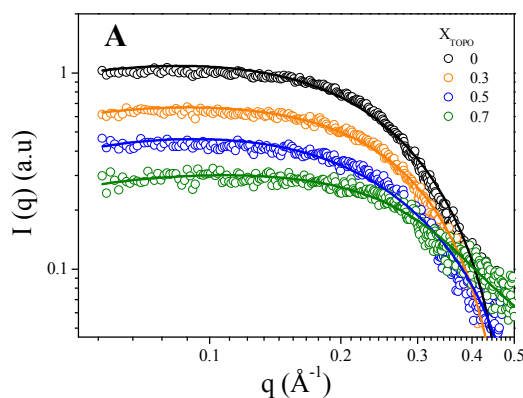


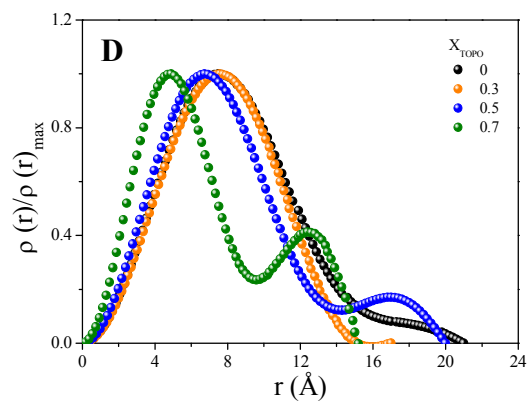
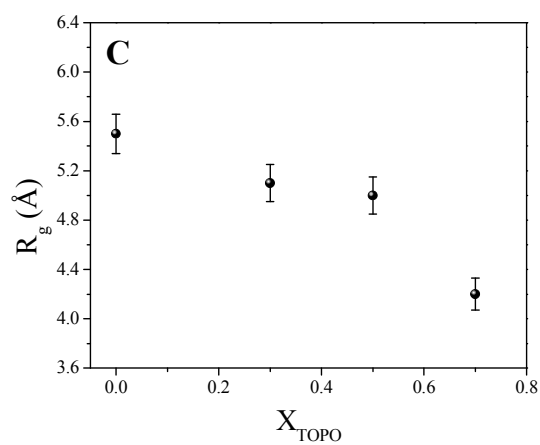
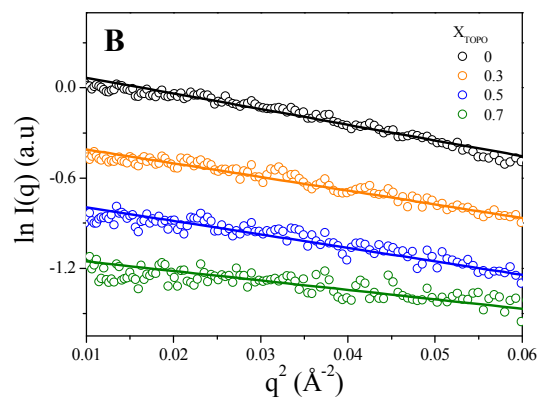
Figure 1. Maximum amount of water solubilized (W_0^{max}) in AOT:TOPO/ML mixed systems as a function of X_{TOPO} . $[\text{Surf.}]_T=0.1$ M.

The water solubilization capacities of RMs are determined by two phenomenological parameters such as the spontaneous curvature and the elasticity of the interfacial film, which are influenced by the constituents of the systems and the experimental conditions.^{37,38} In order to understand the factors that control the water solubilization capacity in these biocompatible systems, we performed SAXS experiments and we also take advantage of the solvatochromic behavior of a molecular probe sensible to different interfacial properties, results shown later in the work. A question may arise here that whether the water is effectively encapsulated by the surfactants creating a mixed RMs media at every X_{TOPO} investigated. In these sense, SAXS is a powerful technique for the direct structural investigations of the systems with the inner structuration falling in the colloidal domain.^{36,39}

2. Small Angle X-Ray Scattering (SAXS) Studies. SAXS measurements were carried out on the water/AOT:TOPO/ML systems at $W_0=2$ and different X_{TOPO} , where all the systems investigated exist in an isotropic single liquid phase. Figure 2 presents (A) the scattering functions, $I(q)$, (B) the Guinier plot ($\ln I(q)$ vs. q^2), (C) the radius of gyration (R_g) as a function of X_{TOPO} , (D) the resulting pair-distance

1
2
3 distribution functions, $\rho(r)$, and (E) the Kratky plot ($I(q)*q^2$ vs. q). Here, we point out
4
5 that since the chemical compositions of both the hydrocarbon oil and the hydrophobic
6
7 part of the surfactants are similar, SAXS selectively detects the hydrophilic core of the
8
9 RMs. Therefore, $\rho(r)$ must be recognized as a measure of the micellar core
10
11 structure.^{36,40,41} The forward scattering intensity, $I(q \rightarrow 0)$, reaches $q=0$ parallel to q -axis
12
13 for the water/AOT/ML and water/AOT:TOPO/ML systems, indicating the formation of
14
15 spheroid type RMs.^{36,42} For water/AOT:TOPO/ML mixed systems, $I(q)$ in the small q
16
17 region decrease with increasing X_{TOPO} , and in the high q region (or cross-section region)
18
19 it shifts apparently toward the forward direction. These features of the scattering curves
20
21 reflect a decrease in the micellar size with increasing the TOPO content. The R_g are
22
23 shown in Figure 2C, and both R_g and those calculated from the $\rho(r)$ plot ($R_{g,r}$) are listed
24
25 in Table S1 in the SI. Values of comparable magnitude were observed for Zhang et al.³⁶
26
27 for AOT RMs dissolved in analogous friendly oil like IPM at the same W_0 in presence
28
29 of different alcohol types. As can be seen, Figure 2C and the values listed in Table S1
30
31 well reflect the size reduction with increasing TOPO content. The higher amount of
32
33 TOPO at the interface layer produce smaller mixed RMs. Thus, AOT:TOPO/ML mixed
34
35 system can solubilize less water than the AOT/ML RMs, and upon increasing the X_{TOPO}
36
37 value the solubilization capacity of the mixed systems decrease (see Figure 1).
38
39
40
41
42





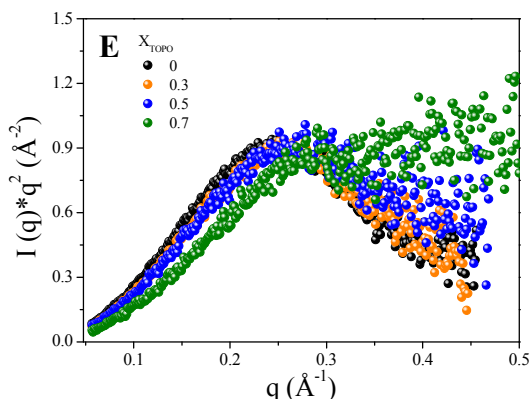


Figure 2. (A) Scattering intensities, $I(q)$, (B) the Guinier plot, (C) the radius of gyration (R_g) as a function of X_{TOPO} , (D) the corresponding normalized pair-distance distribution functions, $\rho(r)/\rho(r)_{\text{max}}$, deduced from the GIFT analysis and (E) the Kratky plot for water/AOT:TOPO/ML mixed RMs at $W_0=2$ and different X_{TOPO} . The solid lines in panel A represent GIFT fit.

The features in reciprocal space are well manifested in the real-space functions in a more intuitive way. In this sense, the $\rho(r)$ function is calculated according to eq (1) and showed in Figure 2D. For water/AOT/ML system, the curve presents a slightly asymmetric bell-shaped peak, suggesting that the RMs has a slightly elongated but nearly spherical shape.^{36,42} The peak apparently shifts to the lower r with increasing X_{TOPO} , indicating the decrease of the micellar size in mixed RMs, which is in good agreement with the results shown in Figure 2A, Figure 2C and Table S1. We can also verify that for higher TOPO content at the region near D_{max} , the distribution curve shows a behavior related to possible interactions between micellar structures that constitute the system, since the curve shows oscillations around this region.⁴³ In this sense, the bell-shaped peak profile accompanies a low hump or shoulders, particularly for $X_{\text{TOPO}} \geq 0.5$, mostly locate twice or thrice distance compared with the positions of the

1
2
3 first maximums in the $\rho(r)$ functions. The maximum peak in the $\rho(r)$ curve can be
4 related to very small structures like discrete droplets, and the shoulder or the low hump
5 peak to larger structures like oligomeric species such as dimers or trimers due the
6 strong interactions between RMs.^{36,44} Thus, this indicates that a large proportion of RMs
7 are discrete droplets with a small proportion of oligomers in the system.
8
9
10
11
12

13 We use the Kratky plot (Figure 2E) to describe a qualitative approach of the
14 structural characteristic such as interfacial fluidity.^{45,46} In the Kratky plot, the scattering
15 curve for RMs with rigid interface exhibits a peak roughly shaped like a parabola. In
16 contrast, RMs with fluid interfaces lack this characteristic peak and the curve profile
17 increases monotonically in the large q region.^{45,46} In these sense, it can be deduced from
18 Figure 2E that the interface of water/AOT/ML RMs is rigid, and the surfactant AOT
19 forms a compact organized system in the biocompatible solvent. When X_{TOPO} content
20 increases, the curve loses progressively its bell-shaped peak suggesting that the nonionic
21 surfactant increases the mixed interfacial fluidity. The presence of the nonionic
22 surfactant shields the AOT head group repulsion making the interface more fluid.^{20,47}
23 The induced fluidity in turn increases the attractive interaction between the droplets,
24 produces shape fluctuations, facilitates clustering of RMs and thereby limits the water
25 solubilization capacity.⁶
26
27
28
29
30
31
32
33
34
35
36
37
38
39
40

41 **3. Spectroscopic Studies of 4-AP**

42 *a. Absorption and Stationary Emission Studies of 4-A.* Figure 3A shows the
43 4-AP absorption spectra by varying the surfactant concentration in the water/AOT/ML
44 pure system at $W_0=2$. As it can be seen, the absorption spectra consist of two bands
45 corresponding to different electronic transitions: (i) the band around 300 nm assigned to
46 the $S_0 \rightarrow S_2$ ($\pi-\pi^*$ S_2 -LE) transition, named B_2 band, and (ii) the band around 350 nm
47 assigned to the $S_0 \rightarrow S_1$ (S_1 -ICT) transition, that we will denote as B_1 band.³¹
48
49
50
51
52
53
54
55
56
57
58
59
60

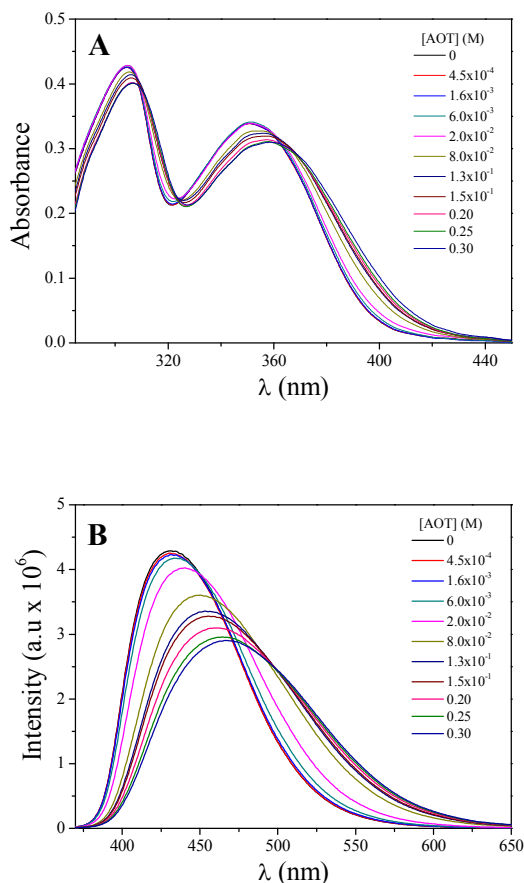


Figure 3. 4-AP absorption (A) and emission (B) spectra in water/AOT/ML pure RMs upon increasing the [AOT] at $W_0=2$. $\lambda_{exc}=350$ nm. $[4-AP]=1 \times 10^{-4}$ M.

In Figure 3A, it is observed also, a small bathochromic shift in the absorption maximum of both bands when the [AOT] increases, being the $\lambda_{max}B_1$ shift greater than for $\lambda_{max}B_2$. Furthermore, there is a slight change in the relative absorption intensity of both bands.

On the other hand, in the emission spectra shown in Figure 3B it can be seen that 4-AP shows a single emission band with maximum emission (λ_{emi}^{max}) at 434 nm in neat ML shifting bathochromically, toward $\lambda_{emi}^{max}=461$ nm, as the surfactant concentration increases. Also, an increase in bandwidth and a decrease in the emission intensity are

observed. Similar emission spectra were recorded for water/AOT:TOPO/ML mixed RMs for different X_{TOPO} at $W_0=0$ and 2 (see Figures S1 and S2, respectively). The decrease in the emission intensity is most likely due to an increase of the internal conversion rate as a consequence of the decrease in the separation between S_1 and S_0 after micellization. The enhancement on the H-bonding with the interfacial water may also be partly responsible for the reduction in fluorescence intensity.⁴⁸ Therefore, the emissive behavior indicates an increase in the interfacial micropolarity due to the polar head solvation. The effect of both the water confinement and the location of the probe can be observed in Figure S3 in the SI, which shows the absorption and the normalized emission spectra of 4-AP in both neat water and pure water/AOT/ML RMs at $W_0=2$. As can be seen, the $\lambda_{\text{emi}}^{\text{max}}$ of 4-AP is 89 nm blue-shifted compared to those in neat water ($\lambda_{\text{emi}}^{\text{max}}=550$ nm),⁴⁹ suggesting that the confined water in water/AOT/ML RMs is substantially less polar than neat water.⁴⁹

Figure S4 in the SI and Figure 4 show the $\lambda_{\text{emi}}^{\text{max}}$ values for 4-AP varying the $[\text{Surf.}]_{\text{T}}$ in water/AOT:TOPO/ML mixed systems at different X_{TOPO} and $W_0=0$ and $W_0=2$, respectively. A progressive red shift of $\lambda_{\text{emi}}^{\text{max}}$ with increasing $[\text{Surf.}]_{\text{T}}$ to ≈ 0.15 M was observed, remaining practically constant above this concentration. The profiles were all sigmoidal in nature and herein employed for critic micellar concentration (cmc) evaluation by fitting them with a Sigmoidal–Boltzmann equation (eq (6)):

$$A = \frac{a_i - a_f}{1 + e^{(x-x_0)/\Delta x}} + a_f \quad (6)$$

where the variable A corresponds to the $\lambda_{\text{emi}}^{\text{max}}$ value, the independent variable (x) is $[\text{Surf.}]_{\text{T}}$, a_i and a_f are the initial and final asymptotes of the sigmoid respectively, x_0 is the center of the sigmoid and Δx is the parameter which characterizes the steepness of

the function. The sigmoidal plot produces cmc value at x_0 ,⁵⁰ and the values for pure and mixed RMs at $W_0=0$ and 2 are listed in Table 1. It is customary to define this concentration value as “operational cmc” (cmc_{op}), since the cmc values depend on the method used to determine it.^{12,51}

As can be seen in Figure 4, the profiles present a smooth variation in the λ_{emi}^{max} as a function of the $[Surf.]_T$. This behavior could reflect self-assembled systems that follow a sequential type association model.¹²

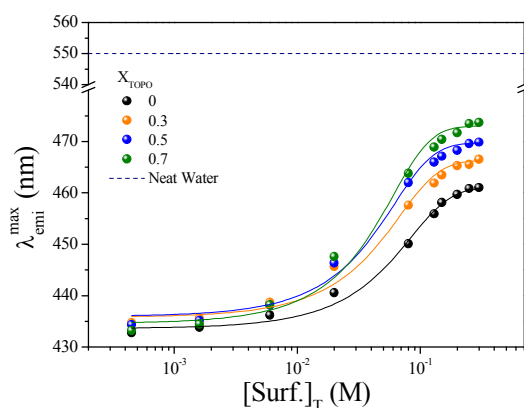


Figure 4. Variation of λ_{emi}^{max} of 4-AP with $[Surf.]_T$ for water/AOT:TOPO/ML mixed RMs at $W_0=2$ and different X_{TOPO} . $\lambda_{exc}=350$ nm. The neat water value (---) is included for comparison.⁴⁹ The solid lines represent the sigmoidal fit using eq (6). $[4-AP]=1 \times 10^{-4}$ M.

The bathochromic shift exhibited in Figure 4 with increasing $[Surf.]_T$ indicates the change in micropolarity of the environment surrounding the probe molecule from the non-polar organic phase to a higher polarity microenvironment provided by the surfactants self-organization. Thus, based on the known behavior of this molecular probe,^{31,52,53} it can be deduced that the micropolarity of the microenvironment sensed by 4-AP increases in comparison to pure ML when the surfactant concentration increases. Indeed, 4-AP emits from two different micro-environments: the organic nonpolar

1
2
3 pseudophase and the pure or mixed RMs interfaces. Hence, it is possible to quantified
4 the partition behavior of 4-AP taking into account the pseudophase model,^{12,54} by means
5 of eq (7) (see calculation procedure of 4-AP partition constants in the SI, section 3 and
6
7 4). In this equation I_0 , $I_{\text{emi}}^{\lambda=430 \text{ nm}}$, ϕ_f , ϕ_b are the incident light, the fluorescence intensity at
8
9 $\lambda_{\text{emi}}^{\text{max}}=430 \text{ nm}$ measured at the surfactant concentration considered, the fluorescent
10
11 quantum yield of 4-AP in the organic solvent and bound to the RM interface (gathered
12
13 in Table S2 of the SI), respectively. Figure 5 shows representative plots of the 4-AP
14
15 emission intensity at $\lambda_{\text{emi}}^{\text{max}}=430 \text{ nm}$ as a function of $[\text{Surf.}]_T$ in the
16
17 water/AOT:TOPO/ML mixed RMs at $W_0=2$ and different X_{TOPO} . The experimental data
18
19 were fitted by eq (7) using a nonlinear regression method and the partition constants
20
21 (K_p) values obtained are gathered in Table 1. The K_p values obtained in different mixed
22
23 RMs at $W_0=0$ are also included.
24
25
26
27
28
29
30

$$I_{\text{emi}}^{\lambda=430 \text{ nm}} = \frac{I_0(\phi_f + \phi_b K_p [\text{Surf.}]_T)}{(1 + K_p [\text{Surf.}]_T)} \quad (7)$$

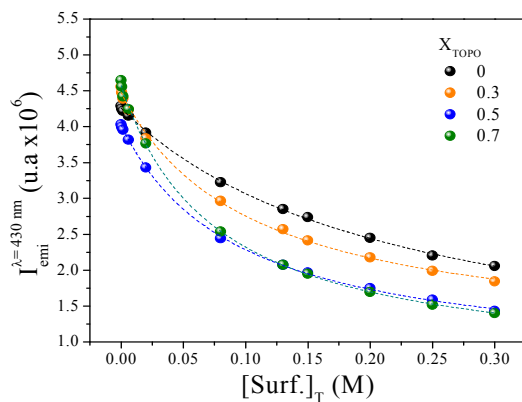


Figure 5. Representative plot of the 4-AP emission intensity at $\lambda_{em}=430$ nm as a function of $[\text{Surf.}]_T$ in the water/AOT:TOPO/ML mixed RMs at $W_0=2$ and at different X_{TOPO} . The data were fitted using eq (7). $[4\text{-AP}]=1 \times 10^{-4}$ M.

Table 1. Operational Critical Micellar Concentration (cmc_{op}), Partition Constants (K_p), and REES ($\Delta\lambda_{emi}^{max}$) Values for 4-AP in Pure and Mixed Water/AOT:TOPO/ML Reverse Micelles at $W_0=0$ and 2

| X_{TOPO} | cmc_{op} (mM) | | K_p (M^{-1}) | | $\Delta\lambda_{emi}^{max}$ (nm) | |
|-------------------|------------------------|------------|--------------------|----------------|----------------------------------|---------|
| | $W_0=0$ | $W_0=2$ | $W_0=0$ | $W_0=2$ | $W_0=0$ | $W_0=2$ |
| 0 | 16 ± 1 | 12 ± 2 | 4.6 ± 1.0 | 4.5 ± 0.3 | 17.4 | 14.0 |
| 0.3 | 15 ± 3 | 10 ± 2 | 8.6 ± 0.8 | 9.7 ± 0.9 | 11.6 | 8.7 |
| 0.5 | 13 ± 2 | 11 ± 1 | 11.4 ± 0.5 | 10.7 ± 0.4 | 8.4 | 5.8 |
| 0.7 | 12 ± 1 | 11 ± 2 | 12.0 ± 0.3 | 13.0 ± 0.8 | 7.6 | 2.6 |

It should be noted that the bathochromic shift is always observed when X_{TOPO} increases at fixed $[\text{Surf.}]_T$ (Figures S4 and 4). Also, this change is magnified once the aggregates are formed ($[\text{Surf.}]_T > \text{cmc}_{op}$). Then we can argue that the probe is capable of monitoring i) an increase in the local micropolarity and/or ii) an increase in the capability to form H-bond interaction between 4-AP and mixed interface. Although TOPO is a nonionic surfactant, the micropolarity sensed by 4-AP increase with TOPO incorporation which might suggest the existence of another factor that have influence on λ_{emi}^{max} . Durantini et. al.³¹ have made the Kamlet-Taft solvatochromic comparison method

(KTSCM) monitoring the frequencies corresponding to the B_1 absorption band and the emission frequencies corresponding to the emission maxima obtained exciting at $\lambda_{\max}B_1$ and $\lambda_{\max}B_2$. The KTSCM parameters obtained from the emission bands at the two monitored excitation wavelength show the same values, and the coefficients that measure the relative sensitivity of the frequencies to the polarity/polarizability (π^*) and H-bond acceptance (or electron pair donation ability to form a coordinated bond, β) are similar.³¹ This implies that 4-AP emission comes from a unique excited state which is affected in equal proportions for both the polarity and the H-bond acceptance or electron pair donation ability of the media. It is interesting to note that, 4-AP does not experiment any effect on its quantum yield when acts as hydrogen bond donor.³¹ Probably, the H-bond interaction of 4-AP is stronger with the TOPO polar head than AOT polar head at the interface. Consequently, this interaction could provide an additional stability of the S_1 -ICT state and have influence on the different emission maxima observed. This behavior is supported from the well-known coordinating features of the phosphorous compound, considering the electronic properties of the trialkyl-substituted P=O group.²⁷⁻³⁰ The fact that there is a bathochromic shift of $\lambda_{\text{emi}}^{\text{max}}$ and a trend towards the value in neat water, would indicate a gradual weakening in the water-mixed interface interaction due TOPO addition. On the other hand, the K_p values increase when the X_{TOPO} increases (see Table 1). Interestingly, not significant changes were observed in K_p values by varying the water content. However, as mentioned above, there is a clear drop in the emission intensity when 4-AP is confined in the mixed RMs at $W_0=2$. The behavior could be only explained taking account the ϕ_b values of the probe at the two different W_0 . As can be seen in the Table S2, the ϕ_b values at $W_0=2$ are almost 4 times lower than the ϕ_b values reported in the systems without water addition ($W_0=0$). This fact shows what is also already known for 4-AP:

1
2
3 the emission quantum yield decreases in solvents which are polar and protic and, much
4 more in water.³¹ Also, from Table S2 it can be seen an independency on the ϕ_b values
5 with the TOPO concentration, which shows that the quantum yield of the molecule is
6 not affected by the hydrogen bond acceptor abilities of the surrounding.³¹ On the other
7 hand, the weak water-mixed interface interaction due to the TOPO addition makes the
8 water/AOT:TOPO/ML mixed RMs interface more fluid than the water/AOT/ML pure
9 RMs, which favors the 4-AP partition toward the RMs pseudophase and explains the
10 increase in K_p . Also, the H-bond interaction between 4-AP and TOPO seems to be a
11 powerful driving force for the molecular probe to reach the mixed RMs interface.
12
13
14
15
16
17
18
19
20
21

22 *b. Red-Edge Excitation Shift (REES) studies.* A direct consequence of
23 organized systems is the restriction imposed on the dynamics and mobility of their
24 constituent structural units. Wavelength-selective fluorescence comprises a set of
25 approaches based on the red edge effect in fluorescence spectroscopy, which can be
26 used to directly monitor the environment and dynamics around a fluorophore in
27 different complex system.⁵⁵⁻⁵⁷ A shift in the wavelength of maximum fluorescence
28 emission toward higher wavelengths, caused by a shift in the excitation wavelength
29 toward the red edge of absorption band, is known as red edge excitation shift (REES)
30 phenomenon.^{57,58} This effect is mostly observed with polar fluorophores in motion
31 restricted media such as very viscous solutions or condensed phases where the dipolar
32 relaxation time of the solvent shell around a fluorophore is comparable to or longer than
33 its fluorescence lifetime.⁵⁷ REES arises from slow rates of solvent relaxation
34 (reorientation) around an excited state of the fluorophore, which is a function of the
35 motional restriction imposed on the solvent molecules in the immediate vicinity of the
36 fluorophore. Utilizing this approach, it becomes possible to probe the mobility
37
38
39
40
41
42
43
44
45
46
47
48
49
50
51
52
53
54
55
56
57
58
59
60

parameters of the environment itself (which is represented by the relaxing solvent molecules) using the fluorophore merely as a reporter group.⁵⁹

An example is shown in Figure S5 for the 4-AP emission spectra, exciting at $\lambda_{\text{exc}}=350$ nm and $\lambda_{\text{exc}}=400$ nm (the red edge of the band), in water/AOT/ML system at $W_0=0$. Identical experiments were made (data not shown) for all the systems studied. For 4-AP, the magnitude of REES ($\Delta\lambda_{\text{emi}}^{\text{max}}$) was defined as the difference in the emission maximum wavelength when exciting at $\lambda_{\text{exc}}=400$ nm and $\lambda_{\text{exc}}=350$ nm at $[\text{Surf.}]_{\text{T}}=0.1$ M: $\Delta\lambda_{\text{emi}}^{\text{max}}=(\lambda_{\text{emi}}^{\text{max}})_{\text{exc}=400 \text{ nm}}-(\lambda_{\text{emi}}^{\text{max}})_{\text{exc}=350 \text{ nm}}$. The Table 1 summarizes the REES values obtained. For AOT pure RMs in water absence ($W_0=0$), the $\Delta\lambda_{\text{emi}}^{\text{max}}=17.4$ nm found reflects the motion constrained environment that 4-AP senses at the interface. Similar results have previously been obtained for this probe in other RMs.⁵⁸ For mixed RMs (see Table 1), the decreases in the REES values with increasing X_{TOPO} , suggest that the interface become progressively more fluid with TOPO incorporation. Upon water addition, it can be seen that for both pure and mixed RMs, the $\Delta\lambda_{\text{emi}}^{\text{max}}$ values decreases suggesting that the dye's environment becomes significantly more fluid due the interface hydration. This phenomena is well known for many RMs^{31,58,59} and corroborates the formation of the systems in the friendly solvent. When comparing systems with the same water content ($W_0=2$), it can be seen that the TOPO incorporation decrease the REES magnitude. The decrease in the translation and rotation dynamics of water molecules interacting strongly with the AOT polar head is one of the causes for the REES effect manifestation.^{31,58,59} From this point of view, the presence of TOPO in the mixed interface would cause the progressive weakening in the water-mixed interface interaction and release of the hydration water, implying the gradual recovery of the polar solvent mobility and the lower REES values observed. This dehydration of the micellar interface is found to be essential for the size control of

1
2
3 micellar aggregates,⁶⁰ and the decrease in the REES effect due to the X_{TOPO} increase
4 supports the RMs size modification (see Figure 2C), the changes observed in the Kratky
5 representations (see Figure 2E) and the partition behavior of 4-AP (see Table 1).
6
7

8
9 4. ³¹P NMR Spectroscopy Studies. In order to gain more insight about the
10 water-surfactants interactions and its impact on the counterions-surfactants interaction
11 at the interface, we investigated the biocompatible mixed RMs using ³¹P NMR
12 spectroscopy. Figure 6 shows ³¹P NMR spectra for pure TOPO/ML and
13 AOT:TOPO/ML systems without and with water as described in Figure caption. The
14 different peak positions of the P=O group of TOPO in homogeneous and micellar media
15 are listed in Table 2. The P=O signal of TOPO/ML system is around $\delta=41.7$ ppm, and
16 undergoes a downfield shift to $\delta=47.0$ ppm with the AOT incorporation (see Figure 6A
17 and Table 2). This behavior is due to the large affinity of TOPO for Na^+ counterions at
18 the interface; the strong interaction between P=O group and Na^+ causes a pronounced
19 decrease in the electron density of the valence orbitals of phosphorus, explaining the
20 downfield shift observed.^{27,30} By contrast, the situation is different when the surfactants
21 are dissolved in polar solvents such as chloroform, where no formation of RMs is
22 observed. Accordingly, the change in the δ is insignificant (see Table 2). Although
23 chloroform is not polar enough, the δ for TOPO/ CDCl_3 and water/AOT:TOPO/ML are
24 quite similar. As shown in our previous work, when the Kamlet-Taft solvatochromic
25 comparison method was performed on the probe 4-AP, we use the following values for
26 chloroform: polarity/polarizability parameter (π^*)=0.58, hydrogen bond acceptance or
27 electron pair donation ability to form a coordinated bond (β)=0.1 and the hydrogen bond
28 donation ability of the solvent (α)=0.44.^{31,61} Since π^* and α parameters have comparable
29 values we believe that chloroform is capable to interact by H-bond interaction with the
30 oxygen present in the TOPO polar head and could explain the similar δ observed for
31
32
33
34
35
36
37
38
39
40
41
42
43
44
45
46
47
48
49
50
51
52
53
54
55
56
57
58
59
60

both the system TOPO/ CDCl_3 -without self-organization- and mixed water/AOT:TOPO/ML. When water is incorporated in TOPO/ML system (Figure 6B), the P=O signal appears at $\delta=43.4$ ppm, 1.7 ppm downfield compared with the value observed in absence of water.

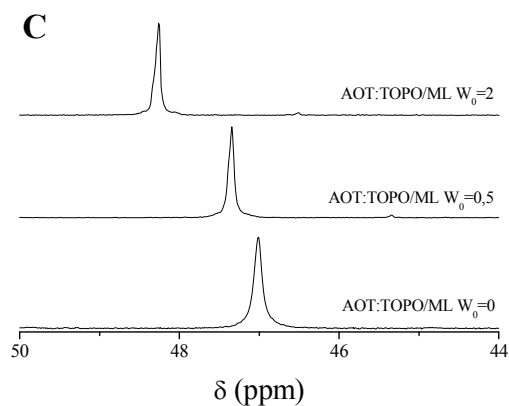
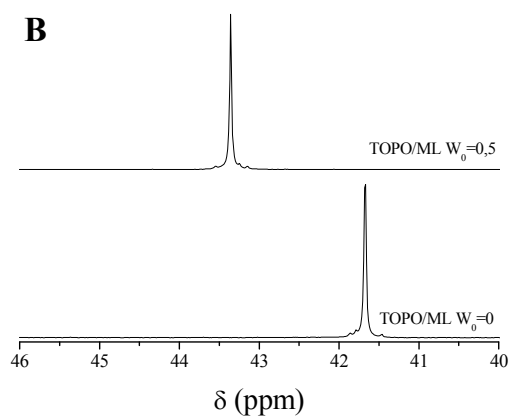
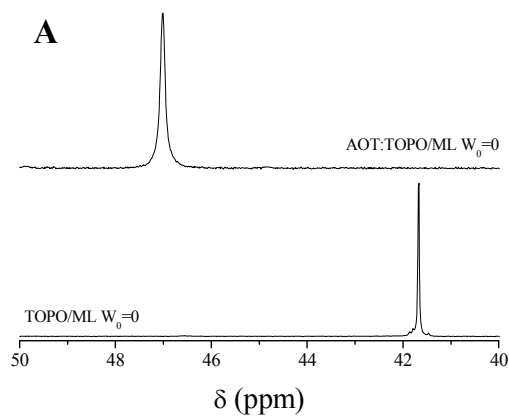


Figure 6. ^{31}P NMR spectra for (A) TOPO/ML pure and AOT:TOPO/ML ($X_{\text{TOPO}}=0.5$) mixed systems at $W_0=0$, (B) water/TOPO/ML pure system at different W_0 ($W_0=0$ and 0.5), and (C) water/AOT:TOPO/ML ($X_{\text{TOPO}}=0.5$) mixed systems at different W_0 ($W_0=0$, 0.5 and 2).

Table 2. ^{31}P NMR Chemical Shifts of P=O Group for TOPO in Homogeneous and Micellar Media

| <i>Systems</i> | X_{TOPO} | W_0 | <i>Chemical Shift (ppm)</i> |
|---------------------------|-------------------|-------|-----------------------------|
| TOPO/ CDCl_3 | 1 | 0 | 47.9 ^a |
| AOT:TOPO/ CDCl_3 | 0.5 | 0 | 47.8 ^a |
| TOPO/ML | 1 | 0 | 41.7 |
| water/TOPO/ML | 1 | 0.5 | 43.4 |
| AOT:TOPO/ML | 0.5 | 0 | 47.0 |
| water/AOT:TOPO/ML | 0.5 | 0.5 | 47.3 |
| water/AOT:TOPO/ML | 0.5 | 2 | 48.3 |

^a δ values obtained from ref. [27].

On the other hand, there is a slight downfield shift in the P=O signal upon increasing the W_0 in the mixed RMs (Figure 6C). At $W_0=0.5$, the P=O signal shift only 0.3 ppm downfield than the value at $W_0=0$ ($\delta=47.0$ ppm). Moreover, when water is encapsulated in small quantities into mixed RMs, the difference in the chemical shift is about 6 times less than the observed in the pure TOPO/ML system ($\Delta\delta=1.7$ ppm, see Table 2). This means that the water-mixed interface interactions are weaker than the water-pure AOT RMs interface interactions at very low W_0 values.

CONCLUSION

In the present study, we demonstrate the existence of pure AOT and mixed AOT:TOPO self-organized assemblies dispersed in non-toxic ML medium. When the X_{TOPO}

1
2
3 increases, the water solubilization capacity diminishes dramatically. SAXS curves
4
5 reflect a decrease in the micellar size with increasing the TOPO content. Also, the
6
7 analysis of the $\rho(r)$ function confirm the very small structures like discrete droplets with
8
9 nearly spherical shape, slightly elongated, and shows larger structures like oligomeric
10
11 species at higher TOPO content in the micellar solution. Furthermore, the nonionic
12
13 surfactant increases notably the mixed interfacial fluidity. The overall behaviors were
14
15 rationalized in terms of the great activity of the nonionic surfactant at the micellar
16
17 interface and the increase of the effective packing parameter. On the other hand, the
18
19 molecular probe 4-AP sense i) an increase in the local micropolarity and/or ii) an
20
21 increase in the capability to form H-bond interaction between 4-AP and the mixed
22
23 interface when TOPO is incorporated. Furthermore, the probe undergoes REES effect
24
25 when is dissolved in the biocompatible RMs, and the decreases in the REES values with
26
27 increasing X_{TOPO} confirm the increase of the interfacial fluidity by TOPO incorporation.
28
29 It is important to note that the water-mixed interface interactions are weaker than the
30
31 water-pure AOT interface interactions as suggested by the solvatochromic behavior of
32
33 4-AP and confirmed by ^{31}P NMR experiments.
34
35
36

37 We demonstrate that adding the nonionic TOPO surfactant into the AOT RMs
38
39 produce remarkable changes at interfacial level, having control on the size, the
40
41 interfacial fluidity and the water-mixed interface interactions, properties that were
42
43 characterized in the work. In particular, both SAXS experiments and REES experienced
44
45 by the probe 4-AP can be used together to understand the variations of the interfacial
46
47 fluidity, property that become difficult to measure directly inside RMs.
48
49

50 Several properties of the mixed RMs studied here are similar to those previously
51
52 reported for the surfactants mixture dissolved in n-heptane. However, those peculiar
53
54 features take place in a biocompatible solvent such as ML, and the environmentally
55
56
57
58
59
60

friendly AOT:TOPO mixed RMs generated could be a promissory alternative in the green synthesis of nanoparticles using the RMs methodology.

Acknowledgments

Financial support from the Consejo Nacional de Investigaciones Científicas y Técnicas (PIP CONICET 112-201101-00204, PIP CONICET 112-2015-0100283), Universidad Nacional de Río Cuarto (PPI-UNRC 2016-2018), Agencia Nacional de Promoción Científica y Técnica (PICT 2012-0232, PICT 2015-0585 and PICT-2015-2151), and Ministerio de Ciencia y Tecnología, gobierno de la provincia de Córdoba (PID 2013) is gratefully acknowledged. E. O. is now a postdoctoral associate at Arizona State University. R. D. F., M. C., J. J. S. and N. M. C. are staff members of CONICET, Argentina.

SUPPORTING INFORMATION

Supporting Information Available; Section 1: Additional Figures and Tables from the main manuscript; Section 2: General procedure and instrumentation for ^{31}P NMR, steady state absorption and emission spectroscopy; Section 3: Calculation procedure of K_p ; Section 4: 4-AP fluorescence quantum yield determination in ML. This material is available free of charge via the Internet at <http://pubs.acs.org>.

REFERENCES

- (1) Bardhan, S.; Kundu, K.; Kar, B.; Chakraborty, G.; Ghosh, D.; Sarkar, D.; Das, S.; Senapati, S.; Saha, S. K.; Paul, B. K. Synergistic Interactions of Surfactant Blends in Aqueous Medium Are Reciprocated in Non-Polar Medium with Improved Efficacy as a Nanoreactor. *RSC Adv.* **2016**, *6*, 55104–55116.

- 1
2
3 (2) Tang, L. L.; Ryabov, A. D.; Collins, T. J. Kinetic Evidence for Reactive Dimeric
4 TAML Iron Species in the Catalytic Oxidation of NADH and a Dye by O₂ in
5 AOT Reverse Micelles. *ACS Catal.* **2016**, *6*, 3713–3718.
6
7
8
9 (3) Silva, O. F.; de Rossi, R. H.; Correa, N. M. The Hydrolysis of Phenyl
10 Trifluoroacetate in AOT/n-Heptane RMs as a Sensor of the Encapsulated Water
11 Structure. *RSC Adv.* **2015**, *5*, 34878–34884.
12
13
14
15 (4) Moyano, F.; Falcone, R. D.; Mejuto, J. C.; Silber, J. J.; Correa, N. M. Cationic
16 Reverse Micelles Create Water with Super Hydrogen-Bond-Donor Capacity for
17 Enzymatic Catalysis: Hydrolysis of 2-Naphthyl Acetate by α -Chymotrypsin.
18 *Chem. - A Eur. J.* **2010**, *16*, 8887–8893.
19
20
21
22 (5) Shome, A.; Roy, S.; Das, P. K. Nonionic Surfactants: A Key to Enhance the
23 Enzyme Activity at Cationic Reverse Micellar Interface. *Langmuir* **2007**, *23*,
24 4130–4136.
25
26
27
28
29 (6) Das, A.; Parta, A.; Mitra, R. K. Modulation of Anionic Reverse Micellar
30 Interface with Non-Ionic Surfactants Can Regulate Enzyme Activity within the
31 Micellar Waterpool. *Colloid Polym. Sci.* **2016**, 1–12.
32
33
34
35 (7) Moya-Ramírez, I.; García-Román, M.; Fernández-Arteaga, A. Waste Frying Oil
36 Hydrolysis in a Reverse Micellar System. *ACS Sustain. Chem. Eng.* **2016**, *4*,
37 1025–1031.
38
39
40
41 (8) Adlercreutz, P. Immobilisation and Application of Lipases in Organic Media.
42 *Chem. Soc. Rev.* **2013**, *42*, 6406–6436.
43
44
45
46 (9) Solanki, J. N.; Murthy, Z. V. P. Controlled Size Silver Nanoparticles Synthesis
47 with Water-in-Oil Microemulsion Method: A Topical Review. *Ind. Eng. Chem.*
48 *Res.* **2011**, *50*, 12311–12323.
49
50
51
52 (10) Ganguli, A. K.; Ganguly, A.; Vaidya, S. Microemulsion-Based Synthesis of
53
54
55
56
57
58
59
60

- 1
2
3 Nanocrystalline Materials. *Chem. Soc. Rev.* **2010**, *39*, 474–485.
- 4
5 (11) Correa, N. M.; Silber, J. J.; Riter, R. E.; Levinger, N. E. Nonaqueous Polar
6
7 Solvents in Reverse Micelle Systems. *Chem. Rev.* **2012**, *112*, 4569–4602.
- 8
9 (12) Silber, J. J.; Biasutti, A.; Abuin, E.; Lissi, E. Interactions of Small Molecules
10
11 with Reverse Micelles. *Adv. Colloid Interface Sci.* **1999**, *82*, 189–252.
- 12
13 (13) Lépori, C. M. O.; Correa, N. M.; Silber, J. J.; Falcone, R. D. How the Cation 1-
14
15 Butyl-3-Methylimidazolium Impacts the Interaction between the Entrapped
16
17 Water and the Reverse Micelle Interface Created with an Ionic Liquid-like
18
19 Surfactant. *Soft Matter* **2016**, *12*, 830–844.
- 20
21
22 (14) Liu, D.-E.; Han, H.; Lu, H.; Wu, G.; Wang, Y.; Ma, J.; Gao, H. Synthesis of
23
24 Amphiphilic Polyaspartamide Derivatives and Construction of Reverse Micelles.
25
26 *RSC Adv.* **2014**, *4*, 37130–37137.
- 27
28 (15) Rao, K. S.; Gehlot, P. S.; Trivedi, T. J.; Kumar, A. Self-Assembly of New
29
30 Surface Active Ionic Liquids Based on Aerosol-OT in Aqueous Media. *J. Colloid*
31
32 *Interface Sci.* **2014**, *428*, 267–275.
- 33
34
35 (16) Chatzidaki, M. D.; Papavasileiou, K. D.; Papadopoulos, M. G.; Xenakis, A.
36
37 Reverse Micelles As Antioxidant Carriers: An Experimental and Molecular
38
39 Dynamics Study. *Langmuir* **2017**, *33*, 5077–5085.
- 40
41 (17) Goswami, D.; Basu, J. K.; De, S. Lipase Applications in Oil Hydrolysis with a
42
43 Case Study on Castor Oil: A Review. *Crit. Rev. Biotechnol.* **2013**, *33*, 81–96.
- 44
45 (18) Girardi, V. R.; Silber, J. J.; Correa, N. M.; Falcone, R. D. The Use of Two Non-
46
47 Toxic Lipophilic Oils to Generate Environmentally Friendly Anionic Reverse
48
49 Micelles without Cosurfactant. Comparison with the Behavior Found for
50
51 Traditional Organic Non-Polar Solvents. *Colloids Surfaces A Physicochem. Eng.*
52
53 *Asp.* **2014**, *457*, 354–362.
- 54
55
56
57
58
59
60

- 1
2
3 (19) Gupta, S.; Moulik, S. P. Biocompatible Microemulsions and Their Prospective
4 Uses in Drug Delivery. *J. Pharm. Sci.* **2008**, *97*, 22–45.
5
6
7 (20) Kundu, K.; Das, A.; Bardhan, S.; Chakraborty, G.; Ghosh, D.; Kar, B.; Saha, S.
8 K.; Senapati, S.; Mitra, R. K.; Paul, B. K. The Mixing Behaviour of Anionic and
9 Nonionic Surfactant Blends in Aqueous Environment Correlates in Fatty Acid
10 Ester Medium. *Colloids Surfaces A Physicochem. Eng. Asp.* **2016**, *504*, 331–342.
11
12
13 (21) Kundu, K.; Paul, B. K. Physicochemical Investigation of Biocompatible Mixed
14 Surfactant Reverse Micelles: III. Aqueous NaCl Solubilization, Thermodynamic
15 Parameters of Desolubilization Process and Conductometric Studies. *J.*
16 *Surfactants Deterg.* **2013**, *16*, 865–879.
17
18
19 (22) Boonme, P.; Krauel, K.; Graf, A.; Rades, T.; Junyaprasert, V. B. Characterization
20 of Microemulsion Structures in the Pseudoternary Phase Diagram of Isopropyl
21 palmitate/water/Brij 97:1-Butanol. *AAPS PharmSciTech* **2006**, *7*, E99–E104.
22
23
24 (23) Bumajdad, A.; Eastoe, J.; Nave, S.; Steytler, D. C.; Heenan, R. K.; Grillo, I.
25 Compositions of Mixed Surfactant Layers in Microemulsions Determined by
26 Small-Angle Neutron Scattering. *Langmuir* **2003**, *19*, 2560–2567.
27
28
29 (24) Li, Q.; Li, T.; Wu, J. Comparative Study on the Structure of Reverse Micelles. 2.
30 FT-IR, ¹H NMR, and Electrical Conductance of H₂O/AOT/NaDEHP/n-Heptane
31 Systems. *J. Phys. Chem. B* **2000**, *104*, 9011–9016.
32
33
34 (25) Chatterjee, S.; Nandi, S.; Bhattacharya, S. C. Interface of AOT/Igepal
35 CO720/cyclohexane/water Mixed Reverse Micelle by Spectroscopic Approach.
36 *Colloids Surfaces A Physicochem. Eng. Asp.* **2006**, *279*, 58–63.
37
38
39 (26) Bardhan, S.; Kundu, K.; Das, S.; Poddar, M.; Saha, S. K.; Paul, B. K. Formation,
40 Thermodynamic Properties, Microstructures and Antimicrobial Activity of Mixed
41 Cationic/non-Ionic Surfactant Microemulsions with Isopropyl Myristate as Oil. *J.*
42
43
44
45
46
47
48
49
50
51
52
53
54
55
56
57
58
59
60

- 1
2
3 *Colloid Interface Sci.* **2014**, *430*, 129–139.
- 4
5 (27) Odella, E.; Falcone, R. D.; Silber, J. J.; Correa, N. M. Nanoscale Control Over
6
7 Interfacial Properties in Mixed Reverse Micelles Formulated by Using Sodium
8
9 1,4-Bis-2-Ethylhexylsulfosuccinate and Tri-N-Octyl Phosphine Oxide
10
11 Surfactants. *ChemPhysChem* **2016**, *17*, 2407–2414.
- 12
13 (28) Pecheur, O.; Dourdain, S.; Guillaumont, D.; Rey, J.; Guilbaud, P.; Berthon, L.;
14
15 Charbonnel, M. C.; Pellet-Rostaing, S.; Testard, F. Synergism in a
16
17 HDEHP/TOPO Liquid–Liquid Extraction System: An Intrinsic Ligands
18
19 Property? *J. Phys. Chem. B* **2016**, *120*, 2814–2823.
- 20
21 (29) Rey, J.; Dourdain, S.; Berthon, L.; Jestin, J.; Pellet-Rostaing, S.; Zemb, T.
22
23 Synergy in Extraction System Chemistry: Combining Configurational Entropy,
24
25 Film Bending, and Perturbation of Complexation. *Langmuir* **2015**, *31*, 7006–
26
27 7015.
- 28
29 (30) Odella, E.; Falcone, R. D.; Silber, J. J.; Correa, N. M. How TOPO Affects the
30
31 Interface of the Novel Mixed water/AOT:TOPO/n-Heptane Reverse Micelles:
32
33 Dynamic Light Scattering and Fourier Transform Infrared Spectroscopy Studies.
34
35 *Phys. Chem. Chem. Phys.* **2014**, *16*, 15457–15468.
- 36
37 (31) Durantini, A. M.; Falcone, R. D.; Anunziata, J. D.; Silber, J. J.; Abuin, E. B.;
38
39 Lissi, E. A.; Correa, N. M. An Interesting Case Where Water Behaves as a
40
41 Unique Solvent. 4-Aminophthalimide Emission Profile to Monitor Aqueous
42
43 Environment. *J. Phys. Chem. B* **2013**, *117*, 2160–2168.
- 44
45 (32) Wetzler, D. E.; Chesta, C.; Fernández-Prini, R.; Aramendía, P. F. Dynamic
46
47 Solvation of Aminophthalimides in Solvent Mixtures. *J. Phys. Chem. A* **2002**,
48
49 *106*, 2390–2400.
- 50
51 (33) Maciejewski, A.; Kubicki, J.; Dobek, K. The Origin of Time-Resolved Emission
52
53
54
55
56
57
58
59
60

- 1
2
3 Spectra (TRES) Changes of 4-Aminophthalimide (4-AP) in SDS Micelles. The
4 Role of the Hydrogen Bond between 4-AP and Water Present in Micelles. *J.*
5 *Phys. Chem. B* **2003**, *107*, 13986–13999.
6
7
8
9 (34) David, G.; Pérez, J. Combined Sampler Robot and High-Performance Liquid
10 Chromatography: A Fully Automated System for Biological Small-Angle X-Ray
11 Scattering Experiments at the Synchrotron SOLEIL SWING Beamline. *J. Appl.*
12 *Crystallogr.* **2009**, *42*, 892–900.
13
14
15
16 (35) Glatter, O. Small Angle Scattering and Light Scattering. In *Neutron, X-ray and*
17 *light scattering*; Linder, P., Zemb, T., Eds.; Elsevier Science: New York, 1991; p
18 33–60.
19
20
21
22 (36) Zhang, X.; Chen, Y.; Liu, J.; Zhao, C.; Zhang, H. Investigation on the Structure
23 of Water/AOT/IPM/Alcohols Reverse Micelles by Conductivity, Dynamic Light
24 Scattering, and Small Angle X-Ray Scattering. *J. Phys. Chem. B* **2012**, *116*,
25 3723–3734.
26
27
28
29 (37) Leung, R.; Shah, D. O. Solubilization and Phase Equilibria of Water-in-Oil
30 Microemulsions: II. Effects of Alcohols, Oils, and Salinity on Single-Chain
31 Surfactant Systems. *J. Colloid Interface Sci.* **1987**, *120*, 330–344.
32
33
34
35 (38) Leung, R.; Shah, D. O. Solubilization and Phase Equilibria of Water-in-Oil
36 Microemulsions. *J. Colloid Interface Sci.* **1987**, *120*, 320–329.
37
38
39
40 (39) Villa, C. C.; Moyano, F.; Ceolin, M.; Silber, J. J.; Falcone, R. D.; Correa, N. M.
41 A Unique Ionic Liquid with Amphiphilic Properties That Can Form Reverse
42 Micelles and Spontaneous Unilamellar Vesicles. *Chem. Eur. J.* **2012**, *18*, 15598–
43 15601.
44
45
46
47 (40) Shrestha, L. K.; Sato, T.; Aramaki, K. Intrinsic Parameters for Structural
48 Variation of Reverse Micelles in Nonionic Surfactant (Glycerol α -
49
50
51
52
53
54
55
56
57
58
59
60

- 1
2
3 Monolaurate)/oil Systems: A SAXS Study. *Phys. Chem. Chem. Phys.* **2009**, *11*,
4
5 4251.
- 6
7 (41) Smith, G. N.; Brown, P.; James, C.; Kemp, R.; Khan, A. M.; Plivelic, T. S.;
8
9 Rogers, S. E.; Eastoe, J. The Effects of Counterion Exchange on Charge
10
11 Stabilization for Anionic Surfactants in Nonpolar Solvents. *J. Colloid Interface*
12
13 *Sci.* **2016**, *465*, 316–322.
- 14
15 (42) Shrestha, L. K.; Dulle, M.; Glatter, O.; Aramaki, K. Structure of Polyglycerol
16
17 Oleic Acid Ester Nonionic Surfactant Reverse Micelles in Decane: Growth
18
19 Control by Headgroup Size. *Langmuir* **2010**, *26*, 7015–7024.
- 20
21 (43) Lucena, I. L.; Canuto, J. D. S.; Caroni, A. L. P. F.; Fonseca, J. L. C.; Neto, A. A.
22
23 D.; Dantas, T. N. C. Characterization of Nonionic Surfactant Micellar Structures
24
25 in Organic Solvents by Small Angle X-Ray Scattering (SAXS). *Colloids Surfaces*
26
27 *A Physicochem. Eng. Asp.* **2012**, *408*, 48–56.
- 28
29 (44) Hirai, M.; Kawai-Hirai, R.; Sanada, M.; Iwase, H.; Mitsuya, S. Characteristics of
30
31 AOT Microemulsion Structure Depending on Apolar Solvents. *J. Phys. Chem. B*
32
33 **1999**, *103*, 9658–9662.
- 34
35 (45) Ichikawa, S.; Sugiura, S.; Nakajima, M.; Sano, Y.; Seki, M.; Furusaki, S.
36
37 Formation of Biocompatible Reversed Micellar Systems Using Phospholipids.
38
39 *Biochem. Eng. J.* **2000**, *6*, 193–199.
- 40
41 (46) Putnam, C. D.; Hammel, M.; Hura, G. L.; Tainer, J. a. X-Ray Solution Scattering
42
43 (SAXS) Combined with Crystallography and Computation: Defining Accurate
44
45 Macromolecular Structures, Conformations and Assemblies in Solution. *Q. Rev.*
46
47 *Biophys.* **2007**, *40*, 191–285.
- 48
49 (47) Kundu, K.; Paul, B. K. Physicochemical Investigation of Biocompatible Mixed
50
51 Surfactant Reverse Micelles: II. Dynamics of Conductance Percolation,
52
53
54
55
56
57
58
59
60

- 1
2
3 Energetics of Droplet Clustering, Effect of Additives and Dynamic Light
4
5 Scattering Studies. *J. Chem. Thermodyn.* **2013**, *63*, 148–163.
6
7 (48) Saroja, G.; Samanta, A. Polarity of the Micelle-Water Interface as Seen by 4-
8
9 Aminophthalimide, a Solvent Sensitive Fluorescence Probe. *Chem. Phys. Lett.*
10
11 **1995**, *246*, 506–512.
12
13 (49) Datta, A.; Mandal, D.; Pal, S. K.; Das, S.; Bhattacharyya, K. Solvation Dynamics
14
15 in Organized Assemblies, 4-Aminophthalimide in Micelles. *J. Mol. Liq.* **1998**,
16
17 *77*, 121–129.
18
19 (50) Mondal, S.; Ghosh, S. Role of Curcumin on the Determination of the Critical
20
21 Micellar Concentration by Absorbance, Fluorescence and Fluorescence
22
23 Anisotropy Techniques. *J. Photochem. Photobiol. B Biol.* **2012**, *115*, 9–15.
24
25 (51) De, T. K.; Maitra, A. Solution Behaviour of Aerosol OT in Non-Polar Solvents.
26
27 *Adv. Colloid Interface Sci.* **1995**, *59*, 95–193.
28
29 (52) Maciejewski, A.; Kubicki, J.; Dobek, K. Different Sources of 4-
30
31 Aminophthalimide Solvation Dynamics Retardation inside Micellar Systems. *J.*
32
33 *Colloid Interface Sci.* **2006**, *295*, 255–263.
34
35 (53) Krystkowiak, E.; Dobek, K.; Maciejewski, A. Origin of the Strong Effect of
36
37 Protic Solvents on the Emission Spectra, Quantum Yield of Fluorescence and
38
39 Fluorescence Lifetime of 4-Aminophthalimide. *J. Photochem. Photobiol. A*
40
41 *Chem.* **2006**, *184*, 250–264.
42
43 (54) Lissi, E. A.; Engel, D. Incorporation of N-Alkanols in Reverse Micelles in the
44
45 AOT/n-Heptane/water System. *Langmuir* **1992**, *8*, 452–455.
46
47 (55) Sen, P.; Satoh, T.; Bhattacharyya, K.; Tominaga, K. Excitation Wavelength
48
49 Dependence of Solvation Dynamics of Coumarin 480 in a Lipid Vesicle. *Chem.*
50
51 *Phys. Lett.* **2005**, *411*, 339–344.
52
53
54
55
56
57
58
59
60

- 1
2
3 (56) Satoh, T.; Okuno, H.; Tominaga, K.; Bhattacharyya, K. Excitation Wavelength
4 Dependence of Solvation Dynamics in a Water Pool of a Reversed Micelle.
5 *Chem. Lett.* **2004**, *33*, 1090–1091.
6
7
8
9 (57) Chattopadhyay, A.; Mukherjee, S. Fluorophore Environments in Membrane-
10 Bound Probes: A Red Edge Excitation Shift Study. *Biochemistry* **1993**, *32*, 3804–
11 3811.
12
13
14
15 (58) Durantini, A. M.; Darío Falcone, R.; Silber, J. J.; Mariano Correa, N. More
16 Evidence on the Control of Reverse Micelles Sizes. Combination of Different
17 Techniques as a Powerful Tool to Monitor AOT Reversed Micelles Properties. *J.*
18 *Phys. Chem. B* **2013**, *117*, 3818–3828.
19
20
21
22 (59) Chattopadhyay, A.; Mukherjee, S.; Raghuraman, H. Reverse Micellar
23 Organization and Dynamics: A Wavelength-Selective Fluorescence Approach. *J.*
24 *Phys. Chem. B* **2002**, *106*, 13002–13009.
25
26
27
28
29 (60) Sethi, V.; Mishra, J.; Bhattacharyya, A.; Sen, D.; Ganguli, A. K. Hydrotrope
30 Induced Structural Modifications in CTAB/butanol/water/isooctane Reverse
31 Micellar Systems. *Phys. Chem. Chem. Phys.* **2017**, *19*, 22033–22048.
32
33
34
35 (61) Kamlet, M. J.; Abboud, J. L. M.; Abraham, M. H.; Taft, R. W. Linear Solvation
36 Energy Relationships. 23. A Comprehensive Collection of the Solvatochromic
37 Parameters, ρ^* , α , and β , and Some Methods for Simplifying the
38 Generalized Solvatochromic Equation. *J. Org. Chem.* **1983**, *48*, 2877–2887.
39
40
41
42
43
44
45
46
47
48
49
50
51
52
53
54
55
56
57
58
59
60

TOC GRAPHIC

